U. Walzer. Systematization of binary intermetallic compounds. Phys. Status Solidi (b), 162:75-88, 1990

Zentralinstitut für Physik der Erde, Institutsteil Jena[1])

Systematization of Binary Intermetallic Compounds

By

U. WALZER

Norm-conserving pseudopotentials derived from the Dirac equation serve for the derivation of new characteristic quantities. For each chemical element and each electron shell, two characteristic energy and two characteristic spacing quantities are calculated. Therefrom, functions are formed for binary compounds and alloys of type AB. If two each of these functions are plotted in pairs, an arrangement is obtained according to regions with crystals of the same structure type and same space group, of the same melting temperature class etc. This systematics enables one to eliminate unfavourable combinations in the search for specific physical properties. A few results are plotted.

Aus der Dirac-Gleichung hergeleitete normierte Pseudopotentiale dienen zur Herleitung neuer Kenngrößen. Für jedes chemische Element und jede Elektronenschale werden zwei charakteristische Energie- und zwei charakteristische Abstandsgrößen berechnet. Für binäre Verbindungen und Legierungen vom Typ AB werden daraus Funktionen gebildet. Trägt man je zwei dieser Funktionen paarweise auf, so ergibt sich eine Einteilung nach Gebieten mit Kristallen gleichen Strukturtyps und gleicher Raumgruppe, gleicher Schmelztemperaturklasse usw. Diese Systematiken ergeben die Möglichkeit, bei der Suche nach gewünschten physikalischen Eigenschaften ungünstige Kombinationen auszuschalten. Es werden einige Ergebnisse graphisch dargestellt.

1. Introduction

It is the subject of the present paper to derive new charactertistic quantities from relativistic norm-conserving pseudopotentials. These quantities will then be used for predicting physical properties of (1 : 1) binary intermetallic compounds and for a systematization of these compounds. It is the very object of the author to employ these findings in a theory of the chemical composition of planetary cores; it goes without saying that metallurgical applications are also conceivable. Thus, these objectives are actually of a very practical nature; however, starting from the Schrödinger equation or from the Dirac equation, we nevertheless want to introduce as few heuristic assumptions as possible in the course of deductions. As is well known, the Schrödinger equation can be exactly solved only for very simple systems. Therefore, Hartree [1] approximated the wave function ψ for a many-electron system as a product,

$$\psi(\mathfrak{r}_1, \mathfrak{r}_2, \ldots, \mathfrak{r}_N) = \psi_1(\mathfrak{r}_1)\,\psi_2(\mathfrak{r}_2) \ldots \psi_N(\mathfrak{r}_N)\,. \tag{1}$$

Each of these ψ_i is obtained as the solution of a one-electron Schrödinger equation. The potential contained therein is the result of the addition of the potentials due to the nuclei and that of the other electrons, which results from Poisson's equation. If not all of the ψ_i's are equal, this statement neglects the exchange of electrons, and we will not get a proper arrangement of the energy levels. Fock [2], therefore, has changed this approximation such

[1]) Burgweg 11, O-6900 Jena, FRG.

that the total wave function exhibits the appropriate symmetry behaviour with respect to electron exchange. In this way, a new nonlocal exchange term is created in the Schrödinger equation, so that the Fermi statistics is taken into consideration. At the same time, however, we still use single-particle equations. Correction terms going beyond that, and which are needed for approximating the exact solution of the Schrödinger equation, are designated as correlation terms.

In contrast to these self-consistent-field calculations, the density functional theory [3 to 5] depends to a lesser degree on the configuration of electrons. In the latter theory, it is shown that the total energy E of a system and the quantities which can be derived from it (see, e.g., [6]) can be represented as a function of an integrated quantity, the charge density ϱ. The Thomas-Fermi approach [7] is a special case of the density functional theory. The introduction of first-principle pseudopotentials [8, 9], which were derived from the density functional formalism, constituted a great step forward. They permit, for example, the approximately correct calculation of reflectivity and absorption spectra, band structures, total energies, and structural properties. We are using here the concept of Hamann et al. [10] and the resulting development line of pseudopotentials (Kleinman [11], Bachelet et al. [12], Greenside and Schlüter [13]) for developing our computer programs for the new characteristic quantities.

2. Theory

For the (small) exchange–correlation energy E_{xc} in the local density approximation, we have

$$E_{xc} = \int \mathrm{d}\mathbf{r}\, \varrho(\mathbf{r})\, \varepsilon_{xc}[\varrho(\mathbf{r})]\,. \tag{2}$$

After [14, 15, 12], we use the following approximation for the correlation energy per electron:

$$\varepsilon_c = -0.1432/(1 + 1.0529 r_s^{1/2} + 0.3334 r_s) \quad \text{for} \quad r_s \geqq 1 \tag{3}$$

and

$$\varepsilon_c = -0.0480 + 0.0311 \ln r_s - 0.0116 r_s + 0.0020 r_s \ln r_s \quad \text{for} \quad r_s < 1\,. \tag{4}$$

Let be

$$\varepsilon_x = -0.4582/r_s \tag{5}$$

for the exchange energy per electron.

The relation between ε_{xc} and the charge density ϱ is obtained for the unpolarized gas from

$$\varepsilon_{xc} = \varepsilon_x + \varepsilon_c \tag{6}$$

and

$$\varrho^{-1} = (4\pi/3)\, r_s^3 \tag{7}$$

with all quantities being expressed in atomic units. The other energy contributions can be calculated exactly. After [4], we have for the energy functional

$$E[\varrho] = T_0[\varrho] + \int \mathrm{d}\mathbf{r}\, \varrho(\mathbf{r})\, [V_{ext}(\mathbf{r}) + \tfrac{1}{2}\, \Phi(\mathbf{r})] + E_{xc}[\varrho]\,. \tag{8}$$

T_0 is the kinetic energy for a system without electron–electron interactions, V_{ext} the potential generated by the nuclei, Φ the Coulomb potential generated by the electrons,

$$\Phi(\mathbf{r}) = \int \mathrm{d}\mathbf{r}'\, \frac{\varrho(\mathbf{r}')}{|\mathbf{r} - \mathbf{r}'|}\,. \tag{9}$$

From (8), due to the variational principle, we get

$$\frac{\delta E(\varrho)}{\delta \varrho(\mathfrak{r})} = \frac{\delta T_0}{\delta \varrho(\mathfrak{r})} + V(\mathfrak{r}) = \mu \tag{10}$$

with

$$V(\mathfrak{r}) = \Phi(\mathfrak{r}) + \frac{\delta E_{\mathrm{xc}}[\varrho]}{\delta \varrho(\mathfrak{r})} + V_{\mathrm{ext}}(\mathfrak{r}) \tag{11}$$

and μ the Lagrange multiplier. Now, we only have to solve a single-particle equation for noninteracting particles,

$$[-\tfrac{1}{2}\nabla^2 + V(\mathfrak{r})]\,\psi_i(\mathfrak{r}) = \varepsilon_i \psi_i(\mathfrak{r})\,. \tag{12}$$

The charge density is

$$\varrho(\mathfrak{r}) = \sum_{i=1}^{N} |\psi_i(\mathfrak{r})|^2\,. \tag{13}$$

Since relativistic effects have an influence for the heavier atoms, the Dirac equation is taken as a starting point instead of the Schrödinger equation. For a central potential $V(r)$, this linear matrix equation with first-order partial derivations is simplified such that the following two coupled scalar equations are formed:

$$\frac{\mathrm{d}G_i(r)}{\mathrm{d}r} + \frac{\varkappa}{r} G_i(r) - [2\alpha^{-2} + \varepsilon_i - V(r)]\,\alpha F_i(r) = 0\,, \tag{14}$$

$$\frac{\mathrm{d}F_i(r)}{\mathrm{d}r} - \frac{\varkappa}{r} F_i(r) + [\varepsilon_i - V(r)]\,\alpha G_i(r) = 0\,, \tag{15}$$

F_i is the minor wave-function component; G_i is the major wave-function component. Therefrom, through summation over occupied states i, we obtain the charge density ϱ,

$$\varrho(r) = \sum_{i=1}^{N} [|F_i(r)|^2 + |G_i(r)|^2]\,. \tag{16}$$

The relativistic quantum number $\varkappa$ results from

$$\varkappa = -(l+1) \quad \text{for} \quad j = l + \tfrac{1}{2}$$

and

$$\varkappa = l \qquad \text{for} \quad j = l - \tfrac{1}{2}\,.$$

Atomic units are used throughout the entire paper, that is, $\hbar = m = e = 1$ and $c = \alpha^{-1} = 137.037$.

Neglecting terms of higher order, the two coupled equations (14) and (15) can be summarized as follows outside the core region, with $\varkappa$ being the afore-mentioned relativistic quantum number, l the angular momentum quantum number:

$$\frac{1}{2}\left(\frac{\mathrm{d}^2 G_\varkappa}{\mathrm{d}r^2} - \frac{\varkappa(\varkappa+1)}{r^2} G_\varkappa\right) - (V(r) - \varepsilon)\, G_\varkappa = 0\,. \tag{17}$$

This is the fundamental equation for deducing the pseudopotentials which are based on the principles of [10]:

a) True and pseudo atomic wave functions become identical beyond the core radius r_c.

b) True and pseudo valence eigenvalues are in agreement for a certain atomic configuration.

c) If the integrals from 0 to r are formed for the true and pseudo charge densities, with $r > r_c$, they are found to be in conformity.

d) For $r > r_c$, the logarithmic derivatives of the true and pseudo wave function are in agreement. The same applies to their first energy derivatives.

The transferability achieved by the last two conditions means that the pseudopotentials can be used for both individual atoms and for molecules and solids; the chemical environment, too, does not affect the usability. – The interpolation formulas for the calculation of the exchange-correlation energy from the charge density given above have to be relativistically corrected. To this end, the exchange energy per electron ε_x has to be multiplied by f_ε [16],

$$f_\varepsilon = 1 - (3/2)\{(1+\beta)^{1/2}/\beta - \ln[\beta + (1+\beta^2)^{1/2}]/\beta^2\}^2, \tag{18}$$

where

$$\beta = 0.0140/r_s .$$

The exchange-correlation potential μ_{xc},

$$\mu_{xc} = \frac{d}{d\varrho}[\varrho\varepsilon_{xc}(\varrho)] = \varepsilon_{xc} - \frac{r_s}{3}\frac{d\varepsilon_{xc}}{dr_s}, \tag{19}$$

has to be multiplied by f_μ,

$$f_\mu = -(1/2) + (3/2)\ln[\beta + (1+\beta^2)^{1/2}]/\{\beta(1+\beta^2)\}. \tag{20}$$

The pseudopotentials have to be calculated in five steps:

a) The major wave-function component has to be determined from (17). From it, of course, one can also calculate F_x and a set of one-electron eigenvalues.

b) In the screened full-core potential, the singularity is cut off at the coordinate origin of r.

c) Next, a normalization follows.

d) By inverting the radial Schrödinger equation, the final screened pseudopotentials are created.

e) As a last step, these final screened pseudopotentials are unscreened.

The pseudopotentials thus defined are parametrized. Irrespective of whether one takes the initial parameters α_1, α_2, α_3, C_1, C_2, C_3, C_4, C_5, C_6 from [12] or whether one calculates them anew in the way specified in [17], the following computational scheme suggests itself:

We use a quantity, S_{ikm}, as a starting point for our programming. We define

$$S_{ikm} = \int_0^m dr_1\, r_1^{2+n}\, e^{-(\alpha_i+\alpha_k)r_1^2}. \tag{21}$$

This can be well used as a subroutine because, on the one hand, the error integral is

$$\mathrm{erf}(m) = \frac{2}{\sqrt{\pi}}\int_0^m e^{-r_1^2}\, dr_1 = \frac{2}{\sqrt{\pi}} S_{ikm} \tag{22}$$

if $n = -2$, $\alpha_i = 0$, and $\alpha_k = 1$. On the other hand, the overlap matrix can then be reformulated as follows:

$$S_{ik} = \lim_{m \to \infty} S_{ikm} . \tag{23}$$

The before-mentioned pseudopotential parameters α_j then serve as α_i and α_k, with $\alpha_j = \alpha_{j+3}$ for $j = 1, 2, 3$. If for both indices we have $i \leqq 3$ and $k \leqq 3$, then $n = 0$. If only one of the indices i and k is smaller than or equal to 3, then $n = 2$. If $i > 3$ and $k > 3$, then $n = 4$.

Thus, 21 integrals S_{ik} are obtained for each chemical element and each angular-momentum quantum number l, because $S_{ik} = S_{ki}$. For all elements with an atomic number $Z_a \geqq 22$ and also for some lighter elements, other additional 21 integrals S_{ik} are not negligibly small for a few l. These integrals define the spin–orbit pseudopotential. This is a consequence of relativistic effects. By solving the following equations, we obtain from 21 matrix elements S_{ik} each, 21 matrix elements Q_{ik} each, and through the inverse matrix transformation we get Q_{ik}^{-1}.

$$\begin{aligned}
&Q_{11} = (S_{11})^{1/2} ; \\
&Q_{12} = S_{12}/Q_{11} ; \quad Q_{13} = S_{13}/Q_{11} ; \quad Q_{14} = S_{14}/Q_{11} ; \\
&Q_{15} = S_{15}/Q_{11} ; \quad Q_{16} = S_{16}/Q_{11} ; \\
&Q_{22} = (S_{22} - Q_{12}^2)^{1/2} ; \\
&Q_{23} = (S_{23} - Q_{12}Q_{13})/Q_{22} ; \quad Q_{24} = (S_{24} - Q_{12}Q_{14})/Q_{22} ; \\
&Q_{25} = (S_{25} - Q_{12}Q_{15})/Q_{22} ; \quad Q_{26} = (S_{26} - Q_{12}Q_{16})/Q_{22} ; \\
&Q_{33} = (S_{33} - Q_{13}^2 - Q_{23}^2)^{1/2} ; \\
&Q_{34} = (S_{34} - Q_{13}Q_{14} - Q_{23}Q_{24})/Q_{33} ; \\
&Q_{35} = (S_{35} - Q_{13}Q_{15} - Q_{23}Q_{25})/Q_{33} ; \\
&Q_{36} = (S_{36} - Q_{13}Q_{16} - Q_{23}Q_{26})/Q_{33} ; \\
&Q_{44} = (S_{44} - Q_{14}^2 - Q_{24}^2 - Q_{34}^2)^{1/2} ; \\
&Q_{45} = (S_{45} - Q_{14}Q_{15} - Q_{24}Q_{25} - Q_{34}Q_{35})/Q_{44} ; \\
&Q_{46} = (S_{46} - Q_{14}Q_{16} - Q_{24}Q_{26} - Q_{34}Q_{36})/Q_{44} ; \\
&Q_{55} = (S_{55} - Q_{15}^2 - Q_{25}^2 - Q_{35}^2 - Q_{45}^2)^{1/2} ; \\
&Q_{56} = (S_{56} - Q_{15}Q_{16} - Q_{25}Q_{26} - Q_{35}Q_{36} - Q_{45}Q_{46})/Q_{55} ; \\
&Q_{66} = (S_{66} - Q_{16}^2 - Q_{26}^2 - Q_{36}^2 - Q_{46}^2 - Q_{56}^2)^{1/2} ; \\
&Q_{ik} = 0 \quad \text{for} \quad i > k .
\end{aligned} \tag{24}$$

Using this approach, the components of the orthogonality matrix Q_{ik} were successively determined. In the nonrelativistic case, only one average pseudopotential $\hat{V}_l^{\text{ion}}(r)$ per l occurs. Due to the spin–orbit effect, we observe in the relativistic case a split-up into $\hat{V}_{l+1/2}^{\text{ion}}$ and $\hat{V}_{l-1/2}^{\text{ion}}$,

$$\begin{aligned}
\hat{V}_{l-1/2}^{\text{ion}} &= \hat{V}_l^{\text{ion}}(r) - \frac{l+1}{2} \hat{V}_l^{\text{so}}(r) , \\
\hat{V}_{l+1/2} &= \hat{V}_l^{\text{ion}}(r) + \frac{l}{2} \hat{V}_l^{\text{so}}(r) .
\end{aligned} \tag{25}$$

The curves defined by (25) practically coincide for light elements. For medium-heavy, but particularly for heavy elements, we obtain two distinctly separate curves. The average

pseudopotential $\hat{V}_l^{\text{ion}}$ is obtained as the sum from the core potential

$$\hat{V}_{\text{core}}(r) = -\frac{Z_v}{r}\left\{\sum_{i=1}^{2} C_i^{\text{core}} \operatorname{erf}\left[(\alpha_i^{\text{core}})^{1/2} r\right]\right\} \tag{26}$$

and the short-range l-dependent term

$$\Delta\hat{V}_l^{\text{ion}}(r) = \sum_{i=1}^{3} (A_i + r^2 A_{i+3})\, \mathrm{e}^{-\alpha_l r^2} \tag{27}$$

with the A_i following from (28).

$$\begin{aligned}
A_6 &= -C_6/Q_{66}\,,\\
A_5 &= -(C_5 + Q_{56}A_6)/Q_{55}\,,\\
A_4 &= -(C_4 + Q_{45}A_5 + Q_{46}A_6)/Q_{44}\,,\\
A_3 &= -(C_3 + Q_{34}A_4 + Q_{35}A_5 + Q_{36}A_6)/Q_{33}\,,\\
A_2 &= -(C_2 + Q_{23}A_3 + Q_{24}A_4 + Q_{25}A_5 + Q_{26}A_6)/Q_{22}\,,\\
A_1 &= -(C_1 + Q_{12}A_2 + Q_{13}A_3 + Q_{14}A_4 + Q_{15}A_5 + Q_{16}A_6)/Q_{11}\,.
\end{aligned} \tag{28}$$

$\hat{V}_l^{\text{so}}(r)$ is obtained as given in (27). It defines the strength of spin–orbit effects. The valence charge Z_v and the constants C_i^{core}, α_i^{core}, C_j, and α_j are the parameters of the pseudopotentials. It is obvious that $r = 0$ has to be excluded from (26). One can, however, approximate this value arbitrarily. Various attempts have been made to predict the space group and the structure type of crystals, the melting temperature, and other properties for AB compounds. In these attempts, two phenomenological scales are frequently used for making plots. The characteristic points in these plots are frequently arranged in a systematic manner. Thus, for example, in certain partial regions of the plots, points prevail which define the same crystal structure. Among the quantities plotted on the coordinates we have, e.g., size factors, electronegativity, coordination number, covalent energy gap, ionic energy gap, etc. We want to adopt a different approach in this paper. The author has developed a computational program for calculating the bare-ion pseudopotentials $\hat{V}_{l\pm 1/2}^{\text{ion}}$ according to (25) as a function of r. Both the potentials and the distance r from the centre of the atoms are calculated in atomic units. Depending on the angular momentum quantum number l, we obtain different pseudopotential curves which still split for heavier atoms (spin–orbit splitting). For each curve, a characteristic point was determined as follows: If the potential v has its smallest value for $r = 0$ on the respective curve, we assume that the genuineness $e = 0$. Otherwise, $e = 1$. For $e = 0$, the characteristic pair of numbers r, v defines the point on the curve where $\mathrm{d}^2v/\mathrm{d}r^2 > 0$ and where the curvature k, coming from infinitely large distance r, reaches a maximum for the first time. We have

$$k = \frac{d^2v}{\mathrm{d}r^2}\left[1 + \left(\frac{\mathrm{d}v}{\mathrm{d}r}\right)^2\right]^{-3/2}. \tag{29}$$

For $e = 1$, the characteristic radius r and the characteristic potential v define the first minimum of the curve which is reached coming from the infinite r. In this way, the following quantities were determined for almost all stable elements:

$$\begin{aligned}
&r_{\text{m0}}, v_{\text{m0}}, e_{\text{m0}};\quad r_{\text{m1}}, v_{\text{m1}}, e_{\text{m1}};\quad r_{\text{p1}}, v_{\text{p1}}, e_{\text{p1}};\\
&r_{\text{m2}}, v_{\text{m2}}, e_{\text{m2}};\quad r_{\text{p2}}, v_{\text{p2}}, e_{\text{p2}};\quad r_{\text{m3}}, v_{\text{m3}}, e_{\text{m3}}\,.
\end{aligned}$$

Each of these numerical triples, separated from one another by a semicolon, defines a characteristic point: Radius, pseudopotential, and genuineness. The first index designates the formula used: m means that the first formula has been taken from (25), p designates the second formula from (25). The second index is the angular momentum quantum number. The third index occurring in the description of the diagrams means a label for the sort of atom. For a binary compound, it can be 1 or 2.

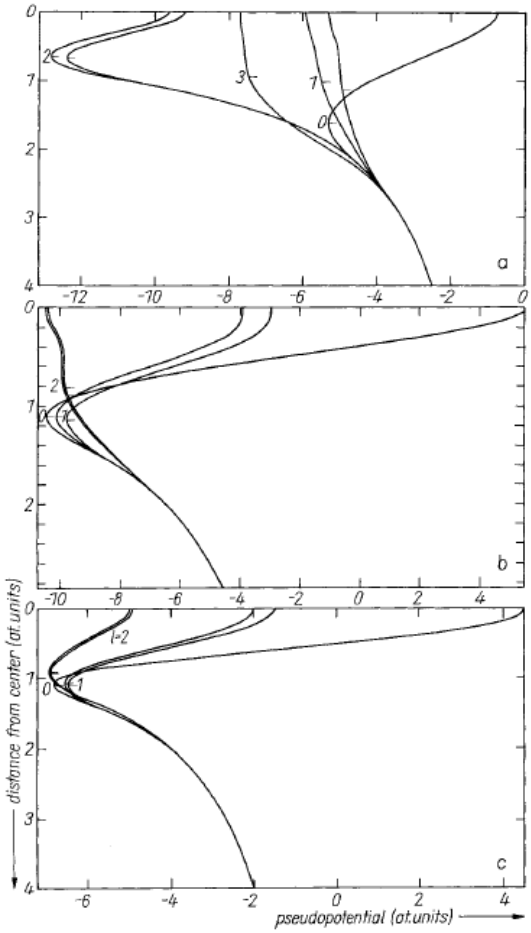

Fig. 1. Pseudopotential curves for a) platinum, b) praseodymium, and c) krypton. For $l = 1$ and $l = 2$, spin–orbit splitting can be clearly seen. The characteristic points which have also been determined by means of a computer are marked

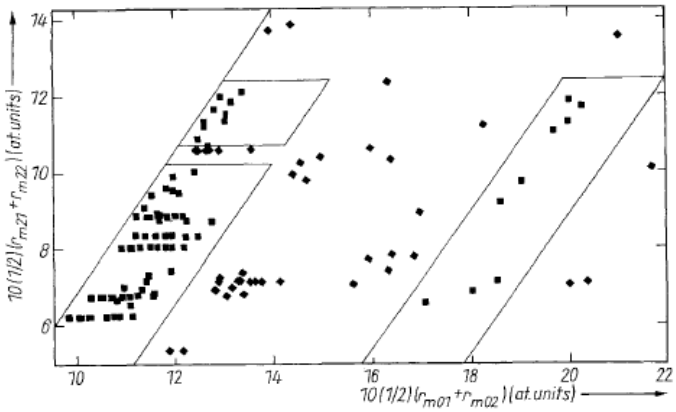

Fig. 2. Radius–radius diagram. The diagram shows (1 : 1) intermetallic compounds of a simple metal and a transition metal each. The following lattices have been selected: Space group $Fm\bar{3}m$ and structure type ClNa (■) and space group $Pm\bar{3}m$ and structure type ClCs (◆) as well as $P6_3/mmc$ (Mg) and $Im\bar{3}m$ (W). The latter ones, however, do not occur in the section

3. Results and Their Diagrammatic Representation

The author has written new computational programs on the basis of the theory briefly outlined above. The pseudopotentials for a noble metal (platinum), a rare-earth element (praseodymium), and a noble gas (krypton) are shown as examples in Fig. 1a to c. The intersection points of the short lines with the curves define the characteristic points, for

Table 1
Symbols for the diagrams in which the symbols represent the space group of the crystal lattice

space group	structure type	symbol
$Fm\bar{3}m$	ClNa	■
$Fm\bar{3}m$	Cu	□
$F\bar{4}3m$	SZn	○
$Fd\bar{3}m$	NaTl	^
$Pm\bar{3}m$	ClCs	◆
$P6_3/mmc$	AsNi	●
$P6_3/mmc$	Mg	◇
$P6_3mc$	SZn	v
Pnma	BFe	▼
Pnma	MnP	▲
P4/mmm	AuCu	◀
P4/nmm	CuTi	▶
$P\bar{4}3n$	GeK	<
$P2_13$	FeSi	>
Cmcm	BCr	+
$Im\bar{3}m$	W	×
$I4_1/acd$	NaPb	*

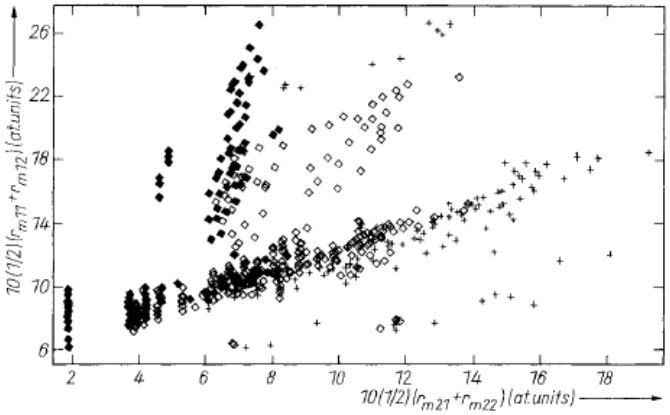

Fig. 3. Radius–radius diagram. ◆ denote compounds and alloys of two transition metals, abbreviated TT. ◇ denote compounds and alloys of transition metal and simple metal, abbreviated ST, + represent those of two simple metals, abbreviated SS. All lattice types were permitted

example, in Fig. 1a from left to right (r_{m2}, v_{m2}), (r_{p2}, v_{p2}), (r_{m3}, v_{m3}), (r_{m1}, v_{m1}), (r_{p1}, v_{p1}) and below (r_{m0}, v_{m0}).

All other diagrams, too, have been prepared by means of a computer. Experimental data have been taken from Pearson's handbook which has been compiled by Villars and Calvert [18]. Not a single value has been eliminated. Table 1 explains the symbols used for Fig. 2 and 5 to 9. In these diagrams, one symbol each is used for the space group and structure type of the crystals. In Fig. 2, we observe a distinct regionalization of the four prevailing lattices.

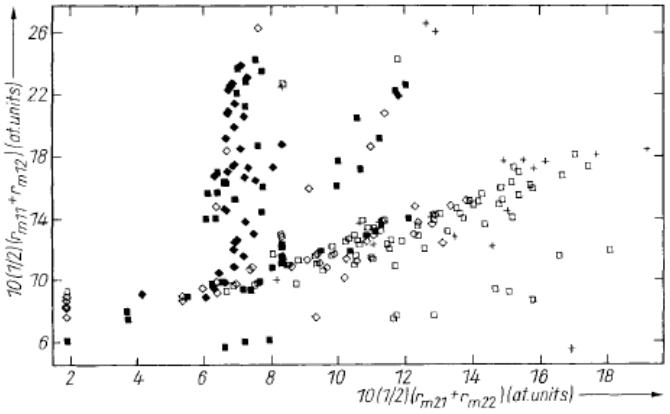

Fig. 4. Radius–radius diagram. ◆ $T_m \geqq 2076$, ■ $2076 > T_m \geqq 1516$, ◇ $1516 > T_m \geqq 956$, □ $956 > T_m \geqq 396$, + $396 > T_m$

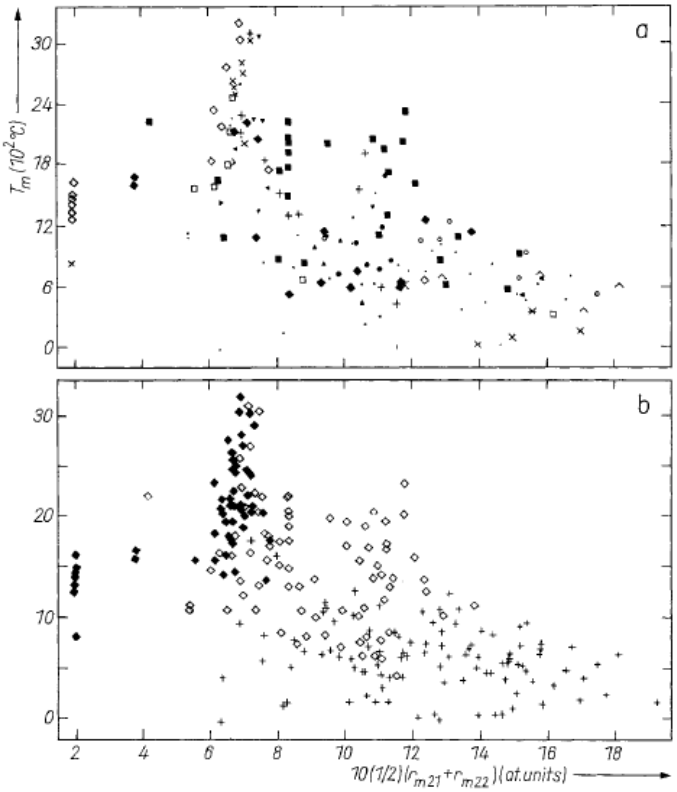

Fig. 5. Radius–melting temperature diagram. a) Symbols as in Table 1, b) with a different meaning of the symbols: ◆ represent compounds and alloys of two transition metals (TT), + those of two simple metals (SS), ◇ correspond to compounds and alloys of a simple metal and a transition metal (ST)

Since the quantities plotted on abscissa and ordinate can be calculated from the theory outlined above, it is also possible to predict the lattice structure for intermetallic compounds that have not yet been produced. In the radius–radius diagram given in Fig. 3, a systematic distribution of the symbols can also be observed. The point clusters TT, ST, and SS are clearly separated particularly for greater radii. The structure of this distribution, however, is by no means simple. Fig. 4 is closely related to Fig. 3. The same quantities are plotted on abscissa and ordinate, but the symbols represent a classification of the melting temperatures as far as they are known. Basically, the TT cloud corresponds to high temperatures, ST to medium, and SS to low temperatures, but for TT with particularly small $10\,(1/2)\,(r_{m21} + r_{m22})$ the melting temperatures are also low. For more details, see the caption. In Fig. 3, we find a number of points, i.e. of intermetallic compounds, which are missing in Fig. 4. In these cases, the experimental melting temperature is not known. In

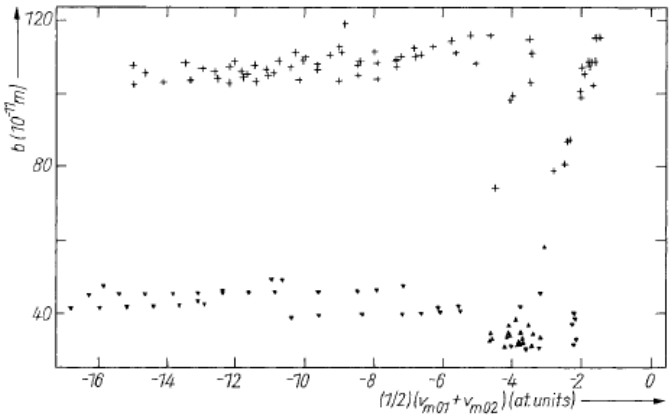

Fig. 6. Potential–lattice constant (b) diagram. Symbols as in Table 1

Fig. 5a, the melting temperature has been plotted versus a kind of transformed d-state radius, namely versus 10 (1/2) ($r_{m21} + r_{m22}$). According to Table 1, the symbols represent the space group of the crystal lattice. For comparison, the related representation in Fig. 5b shows the distribution for TT, ST, and SS. It can be seen that the TT, ST, and SS areas for higher melting temperatures or higher 10 (1/2) ($r_{m21} + r_{m22}$) are located separately from one another. With one exception, the cluster of TT compounds with *very* low values of 10 (1/2) ($r_{m21} + r_{m22}$) belongs to the space group $P6_3/mmc$ and the structure type Mg.

Fig. 6 shows a pseudopotential–lattice constant (b) diagram. Only the three most frequently occurring crystal lattices playing a part in this case are shown. The space group Pnma, linked to the structure type MnP, is observed only on a small area at the right

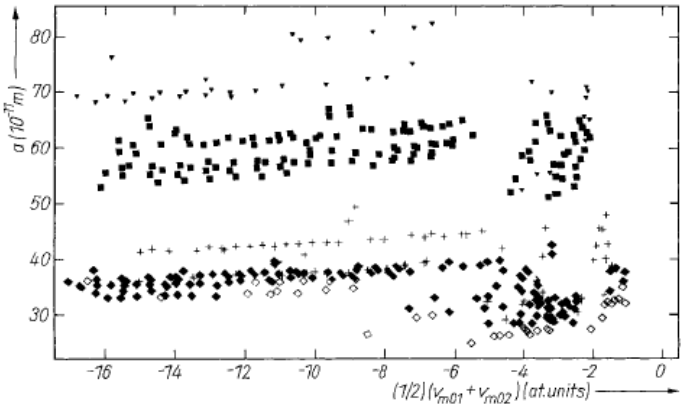

Fig. 7. Potential–lattice constant (a) diagram. Symbols as in Table 1

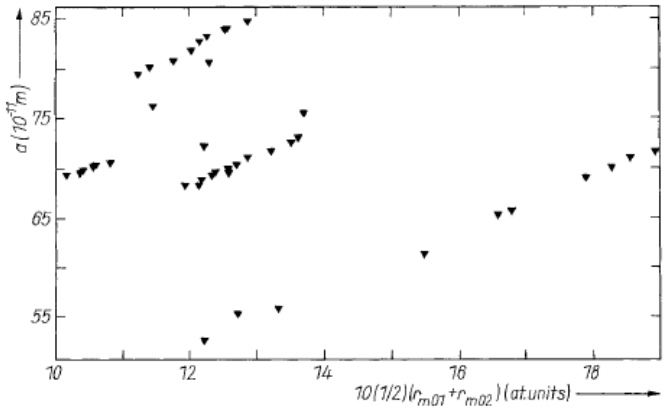

Fig. 8. Radius–lattice constant (a) diagram. Symbols as in Table 1

bottom of the diagram, while for space group Pnma, linked to structure type BFe, as well as for space group Cmcm, linked to structure type BCr, one horizontal ribbon-like area each, and additionally for small absolute amounts of the potential, one vertical ribbon-like area each are found. Fig. 7 is well comparable with Fig. 6. here, the lattice constant a has been plotted versus the same combination of pseudopotentials. The crystal lattices show a comparable arrangement into separate areas, but five types of crystal lattices are prevailing here. In the following enumeration, they are defined each time by the space group and the structure type and separated from one another by semicolons: $Pm\bar{3}m$, ClCs; $Fm\bar{3}m$, ClNa; $P6_3/mmc$, Mg; Cmcm, BCr; Pnma, BFe. In Fig. 8, a radius–lattice constant diagram, only

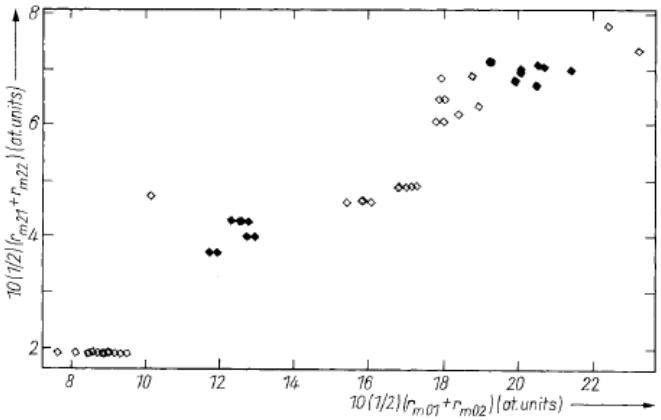

Fig. 9. Radius–radius diagram. Only TT compounds are shown, namely the lattices ($P6_3/mmc$, Mg) and ($Pm\bar{3}m$, ClCs)

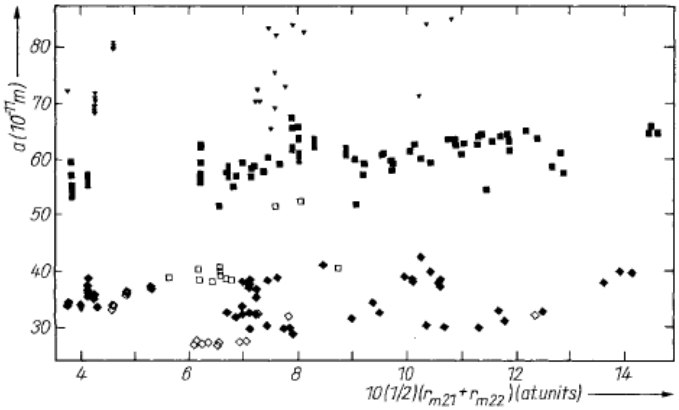

Fig. 10. Radius–lattice constant (a) diagram. Symbols as in Table 1

lattices of space group Pnma and of structure type BFe are shown. The points are arranged here in four lines. The upper short line and the lower long line are formed by (1 : 1) compounds and alloys of type ST, while the two centre lines correspond to type TT. A further systematic arrangement can be observed in Fig. 9. The two radius quantities can be theoretically calculated. The two lattice types ($P6_3/mmc$, Mg) and ($Pm\bar{3}m$, ClCs) are arranged in clusters, so that predictions can be made for the case that the lattice is still unknown. The general distribution of the lattices (see Table 1) is shown in a radius–lattice constant (a) diagram (see Fig. 10). Here, too, individual partial regions of the diagram area are dominated by a certain lattice type.

4. Conclusions

Pseudopotentials that can be derived from the density functional theory have been numerically determined by means of a new computer program. For heavier atomic nuclei, the relativistic spin–orbit splitting of the curves is taken into consideration. For each pseudopotential-spacing curve, one characteristic point is determined. In diagrammatic representations, certain simple combinations of these characteristic quantities lead to the formation of distinct areas, depending on the crystal lattice, melting point, lattice constants, etc. This was observed for binary intermetallic AB compounds and alloys; the method is probably also applicable to other mixture ratios. Thus, the physical quantities studied can be predicted to a certain extent. At any rate, when searching for compounds with specific physical quantities, it is possible to considerably reduce experimental expenditure.

References

[1] D. R. Hartree, Proc. Cambridge Phil. Soc. **24**, 89 (1928).
[2] V. Fock, Z. Phys. **61**, 126 (1930).
[3] P. Hohenberg and W. Kohn, Phys. Rev. **136**, B864 (1964).
[4] W. Kohn and L. J. Sham, Phys. Rev. **140**, A1133 (1965).

[5] M. LEVY, Proc. Nat. Acad. Sci. USA **76**, 6062 (1979).
[6] U. WALZER, phys. stat. sol. (b) **140**, 377 (1987).
[7] E. H. LIEB, Rev. mod. Phys. **53**, 603 (1981).
[8] S. TOPIOL, A. ZUNGER, and M. A. RATNER, Chem. Phys. Letters **49**, 367 (1977).
[9] A. ZUNGER and M. L. COHEN, Phys. Rev. Letters **41**, 53 (1978).
[10] D. R. HAMANN, M. SCHLÜTER, and C. CHIANG, Phys. Rev. Letters **43**, 1494 (1979).
[11] L. KLEINMAN, Phys. Rev. B **21**, 2630 (1980).
[12] G. B. BACHELET, D. R. HAMANN, and M. SCHLÜTER, Phys. Rev. B **26**, 4199 (1982).
[13] H. S. GREENSIDE and M. SCHLÜTER, Phys. Rev. B **28**, 535 (1983).
[14] D. M. CEPERLEY and B. J. ALDER, Phys. Rev. Letters **45**, 566 (1980).
[15] J. PERDEW and A. ZUNGER, Phys. Rev. B **23**, 5048 (1981).
[16] A. H. MACDONALD and S. H. VOSKO, J. Phys. C **12**, 2977 (1979).
[17] U. WALZER, The Application of a Pseudopotential Approach to the Physics of Binary Intermetallic Compounds, High Temp. – High Pressures, in the press.
[18] P. VILLARS and L. D. CALVERT, Pearson's Handbook of Crystallographic Data for Intermetallic Phases, Vol. 1 to 3, Amer. Soc. for Metals, Metals Park (Ohio) 1985.

(Received June 22, 1990)